IEEE Access
Multidisciplinary | Rapid Review | Open Access Journal

Received August 16, 2021, accepted October 12, 2021, date of publication October 15, 2021, date of current version October 29, 2021.

Digital Object Identifier 10.1109/ACCESS.2021.3120741

Real-Time Road Curb and Lane Detection for Autonomous Driving Using LiDAR Point Clouds

JING HUANG[1,2], PALLAB K. CHOUDHURY[3], (Member, IEEE), SONG YIN[1,2], AND LINGYUN ZHU[1]

[1]National Research Center for LiDARs and Intelligent Optical Nodes, Liangjiang International College, Chongqing University of Technology, Chongqing 401135, China
[2]School of Electrical Engineering, Korea Advanced Institute of Science and Technology (KAIST), Daejeon 34141, South Korea
[3]Department of Electronics and Communication Engineering, Khulna University of Engineering & Technology (KUET), Khulna 9203, Bangladesh

Corresponding author: Lingyun Zhu (zhulingyun@cqut.edu.cn)

This work was supported in part by the Banan Science and Technology Foundation of Chongqing, China, under Grant 2018TJ02 and Grant 2020QC430.

ABSTRACT The commercialization of automated driving vehicles promotes the development of safer and more efficient autonomous driving technologies including lane marking detection strategy, which is considered to be the most promising feature in environmental perception technology. To reduce the tradeoff between time consumption and detection precision, we propose a real-time lane marking detection method by using LiDAR point clouds directly. A constrained RANSAC algorithm is applied to select the regions of interest and filter the background data. Further, a road curb detection method based on the segment point density is also proposed to classify the road points and curb points. Finally, an adaptive threshold selection method is proposed to identify lane markings. In this investigation, five datasets are collected from different driving conditions that include the straight road, curved road, and uphill, to test the proposed method. The proposed method is evaluated under different performance metrics such as Precision, Recall, Dice, Jaccard as well as the average detection distance and computation time for the five datasets. The quantitative results show the efficiency and feasibility of this proposed method.

INDEX TERMS Lane marking detection, point cloud, intensity threshold, curb filtering.

I. INTRODUCTION

Recently, self-driving technologies have received much attention due to the several research activities of university-industry collaboration financed by some reputed companies such as Waymo [1] and Hyundai [2]. However, the realization of autonomous driving technology is difficult. The most basic yet important function for an automated vehicle is environmental perception, because of its direct influence on both drivers and pedestrians. Various objects need to be recognized in the procedure of environmental perception, such as lane markings, pedestrians, and adjacent vehicles. Similarly, different sensing modalities are used to achieve autonomous driving, for example, visual and thermal cameras, radars, Light Detection and Ranging (LiDAR) sensors, and ultrasonic sensors. These sensors are equipped alone or combined with others for self-driving vehicles to perceive the driving environment [3]. Among the many targets that need to be perceived, precise lane marking detection is of paramount importance for autonomous vehicles maintaining the advanced driving assistance systems (ADAS), which directly affects the behaviors of driving. Furthermore, the accurate identification of lane markings will be helpful for other transportation applications, such as the localization of vehicles, mobile mapping technology, and optimization of routes. Therefore, lane marking detection is the fundamental feature to develop the autonomous driving system.

Several methods have been proposed to recognize the lane markings from camera images [4], [5]. However, those methods show performance degradation in the acquisition of three-dimensional (3D) information of objects, severe weather conditions, and non-ideal lighting environments [6]. Radar sensors can work even under adverse weather conditions by directly measuring the radial velocity of objects via the

The associate editor coordinating the review of this manuscript and approving it for publication was Yonggang Liu.

Doppler effect. However, the data collected by radar sensors are noisy [7]. The booming of the self-driving industry also promotes the commercialization of LiDAR sensors, because of their ability to offer three-dimensional (3D) information of objects. And more importantly, its operation can continue under different weather and illumination conditions. However, the 3D information increases the processing time and complexity due to the tremendous amount of data, especially due to the multiple (16/32/64) laser scanning system. In order to effectively separate the lane marking points from the LiDAR 3D point clouds, road surface points are first extracted from the raw data, then followed by the differentiation of lane marking points from road clouds.

Usually, approaches of lane marking extraction from LiDAR point cloud can be classified into two categories: two-dimensional (2D) image-based methods, and 3D point cloud-based methods. The first step of 2D image-based methods is converting 3D point clouds to 2D images, then, image processing methods are applied to extract road point clouds. Georeferenced intensity images were interpolated from the road points by Guan *et al.* [8], using an extended inverse distance weighted (IDW) interpolation method, followed by a point-density-based multiple threshold segmentation strategy. Guan *et al.* [9] generated 2D georeferenced feature images (GFI) from 3D road surface points by using a modified IDW interpolation method. After that, the weighted neighboring difference histogram-based dynamic thresholding and multiscale tensor voting algorithms were used to distinguish lane markings from the GFI image. Cheng *et al.* [10] extracted lane markings from thresholding normalized intensity images by using the deep learning approaches. Ma *et al.* [11] first segmented road surface from the raw data by using a revised curb-based road extraction method, followed by the IDW approach for 2D georeferenced image generation. Then, a U-shaped capsule-based network was developed to detect lane markings based on the convolutional and deconvolutional capsule strategies. However, there are some apparent shortcomings of the 2D image-based methods. The conversion from 3D point clouds to 2D images requires powerful abilities of computation because of the immense size of data acquired by a multi-array laser scanning system and corresponding post-processing. Furthermore, such conversion from 3D point clouds to 2D images also suffers in high precision loss, which eventually affects the accuracy of measurement for target objects.

The second type of 3D-based method identifies lane markings from the original point cloud directly, without the procedure of synthesizing point clouds to images. Yu *et al.* [12] proposed a multisegment thresholding and spatial density filtering method to directly extract lane markings after the application of a curb-based road points segmentation approach. Yan *et al.* [13] first eliminated points in the air and organized useful points to scan lines. Subsequently, road points are extracted by the utilization of height difference (HD) and moving least squares line fitting. In the last step, after the smoothness of intensities by a dynamic window median filter, the edge detection and edge constraint methods were operated to identify lane markings. Jung and Bae [14] differentiated drivable regions by setting a vertical slope threshold and discriminated lane markings with higher intensities. Here, the marking points are extracted by searching a set of parallel lines with a fixed interval of lane width. However, most of the methods mentioned previously are used for the generation of digital maps and thus do not directly focus on autonomous driving. Therefore, the design features of such algorithms are quite different in comparison to actual driving conditions. For example, computational time may not an important factor for the generation of digital map, which it has paramount significance for the application in self-driving. Besides, most proposals are based on the assumption that roads are flat and straight. However, the detection of roads with slopes or curvatures would be challenging in practical scenarios.

In this paper, we present a real-time lane marking detection method for structured roads with few obstructions based on a LiDAR sensor using point clouds. Five datasets were collected from different road conditions including slopes or curvature in shape and investigated thoroughly to verify the feasibility of the proposed method. Overall, the main contributions of this paper are as follows:

1) The spatial distribution characteristics of roads are found, which are used to filter background points.
2) A road curb detection algorithm is proposed to classify curbstone points and road points by using the different distribution features of road and curbstones.
3) An adaptive threshold selection method is proposed to distinguish lane marking points from road points by determining a unique threshold for each scan line.
4) The proposed method is tested on five datasets collected from different road conditions including straight roads, curved roads, flat roads, and slopes.

The structure of this paper is as follows: Section 2 presents the features of devices that are used in this research and a brief overview of five different datasets. Approaches of road data segmentation, the proposed curb points filtering and adaptive threshold selection methods are described in Section 3. Experiments, results, and discussion are concluded in Section 4. Finally, Section 5 summarizes the conclusion.

II. DEVICES AND DATASETS

A. DEVICES

In general, researchers choose to use a mobile laser scanning system [8], [9], 64-beam LiDAR [15], [16], or at least 32-beam LiDAR [17], [18] to identify lane markings from point clouds due to its precise 3D information. However, a 16-beam commercial LiDAR is used for this research considering the cost-effective application. The five datasets are captured from five different conditions using the RS-LiDAR-16 sensor mounted on a vehicle about 1.5 meters from the ground, as shown in Fig. 1. As Fig. 1, assume that the origin of LiDAR is the origin of data, the driving direction of the vehicle is the positive direction of the X-axis, the left side

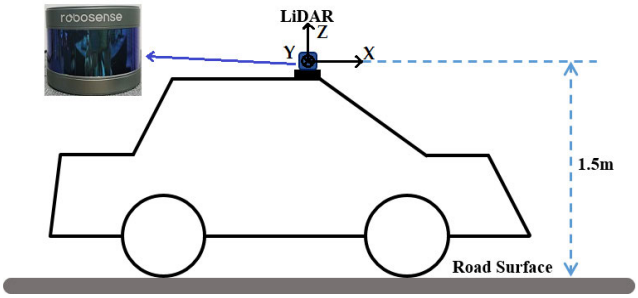

FIGURE 1. The collection devices: a schematic diagram of collection devices and the RS-LiDAR-16.

of driving is the positive direction of the Y-axis, and the vertical direction of the XOY plane is the Z-axis. Fig. 1 also shows the commercial Robosense LiDAR sensor that is used for this investigation. This LiDAR comprises 16 laser and detector pairs with a vertical angular resolution of 2° from −15° to 15° comprising a total vertical field of view of 30°. The detection range is from 20 centimeters to 150 meters long, with a measurement accuracy within ±2 centimeters. The horizontal field of view is 360° with a data rate of 320000 points per second.

B. DATASETS

In this research, five datasets are used to evaluate the performance of the proposed method in different scenarios, such as the straight road, curved road, and uphill, as presented in Fig. 2. The location of the datasets is in Yubei District, Chongqing, China, where the university campus is situated. Road datasets are collected from inside and outside of the campus area, where each of the roads is a couple of kilometers long with diverse scenarios. Dataset 1 is a site of a flat straight road with two white solid lines and a dashed line, while dataset 2 with two white solid lines and a yellow solid line. Dataset 3 is acquired where the road is a straight slope with three white solid lines and one yellow dashed line. The uphill straight road with two white solid lines and a yellow dashed line is also included in this dataset, which is dataset 4. And dataset 5 is a curved and uphill road with two white solid lines and one yellow dashed line. The road slope of dataset 3 is lower than datasets 4 and 5. The exact length of each road and the time of collection are not recorded since we only select 200 frames of data from each dataset. But the number of frames of each of the five datasets are 390, 547, 664, 260, and 239 respectively. This study distinguishes white solid lane markings from 3D point clouds.

III. METHODOLOGY

The workflow of the proposed system is illustrated in Fig. 3. The road surface points are segmented from LiDAR raw data using Random Sample Consensus (RANSAC) algorithm with a plane model [19]. However, some constraints are added to the algorithm in this research and will be discussed in a later section. For the road curb points detection, the rough

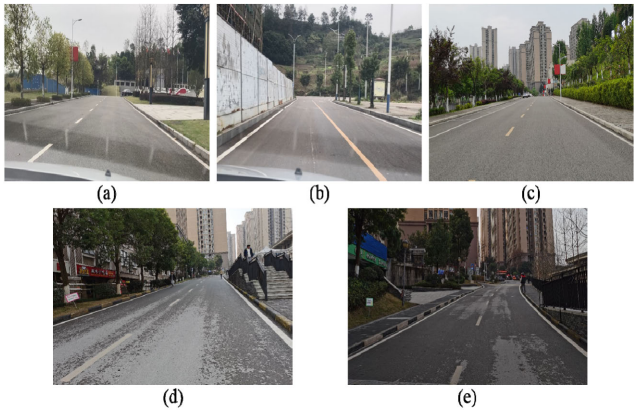

FIGURE 2. Five data collection sites: (a) a flat straight road with two white solid lines and a dashed line, (b) a flat straight road with two white solid lines and a yellow solid line, (c) a straight uphill with 3 white solid lines and a yellow dashed line, (d) a straight uphill with two white solid lines and a yellow dashed line, (e) a curved uphill with two white solid lines and a yellow dashed line.

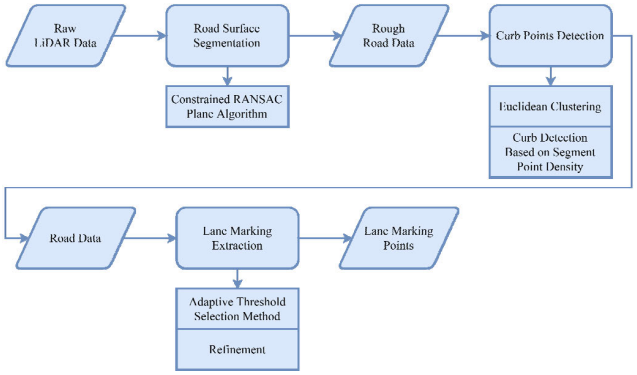

FIGURE 3. The workflow of lane marking detection system.

road data points are clustered using the Euclidean clustering algorithm and further used for curb detection algorithm based on segment point density. Finally, the proposed adaptive threshold selection method including refinement strategy is used to identify lane marking points.

A. REGION-OF-INTEREST-SELECTION

This section introduces those approaches that are adopted to select the region-of-interest (ROI). This selective operation will reduce the computational complexity, which eventually helps to reach the goal of real-time lane marking recognition. There are mainly two subsections: road surface data extraction and curb points detection. The segmentation of raw road point clouds eliminates the majority of useless points, whereas curb detection classifies curb points and road points.

1) EXTRACTION OF ROAD DATA

It is evident that background filtering is crucial for lane marking identification, as the marking points are a small fraction of total point clouds. The RANSAC algorithm is commonly used to extract road data. However, this method

fails when there are more points fall on the pedestrian road than driving road [20]. Therefore, we set some constraints on the RANSAC algorithm. Based on the coordinate system as appeared in Fig. 1(a), the passthrough filter with a specific range of one coordinate is set to either remove or preserve surrounding objects in one frame of data. According to the relation between accuracy and distance of target object based on the user manual of RS-LiDAR-16 [21], the accuracy fluctuates after 70 meters, so the range of the X-axis is set from -70 m to $+70$ m. The threshold of the Y-axis is 10 meters. Then, the original RANSAC algorithm is applied for the ROI selection. This algorithm is reported as the best shape estimation method due to its consideration of slope parameters. First, three points are randomly chosen from point clouds to form a plane model. Then, points that fit this model are retained as inliers, while others are outliers. The number of inliers is recorded and compared between different iterations. In this paper, a distance threshold of 0.07m and iteration number of 200 are experimentally achieved to filter unwanted points and preserve useful points as possible. Finally, the best model is determined by the maximum number of inliers.

So far, the rough road data are extracted from raw LiDAR data, where the constrained RANSAC algorithm cannot remove points of road curb. However, the existence of road curb points will influence lane marking detection, as these have reflectivity higher than asphalt points.

2) CURB POINTS DETECTION

Generally, roads include both structured and unstructured data, and lane markings are only present on structured roads. By observing datasets collected in this study, we found that points are arranged in fan-shaped scan lines on the structured road, and the distance between each arc exceeds at least 0.5 meters as shown in Fig. 4(a). Furthermore, roadside data are dense than road data in a certain horizontal range, which is again confirm through data characteristics as shown in Fig. 4(b). Therefore, this statistical feature is used to filter curb points, and the curb detection algorithm based on segment point density is proposed to refine the extracted road points.

In order to detect curb points, road points are classified into different clusters based on scan lines. Here, points representing different scan lines are decided by the K dimensional tree (Kd-tree) structure with Euclidean distance threshold d_{th} of 0.2 meters. If the radii of neighbor points in a sphere can satisfy the constraint of,

$$r = \sqrt{x^2 + y^2 + z^2} < d_{th} \tag{1}$$

these points are grouped to the same clusters. Later, those clusters are subdivided to several segments by a fixed length of segment *LS* in the Y direction. However, the real length of a segment *RLS* is not equal to *LS* due to the spatial distribution characteristic of points. It is determined by,

$$RLS = y_{\max} - y_{\min} \tag{2}$$

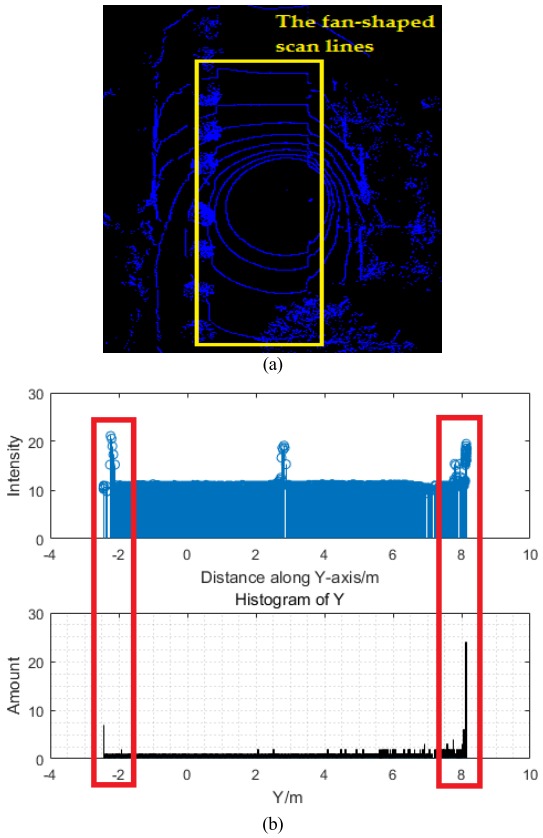

FIGURE 4. Diagrams of data characteristics: (a) data feature of structured roads, (b) statistical features.

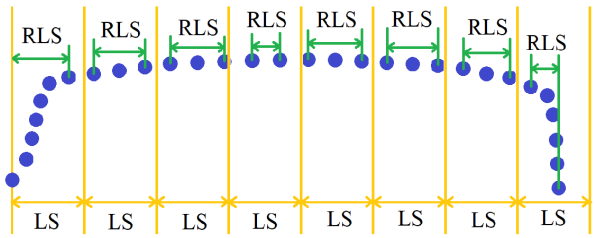

FIGURE 5. A schematic diagram of the difference between LS and RLS: blue points are points on one scan line, the distance divided by the yellow line is LS, and the distance marked by the green line is RLS.

where, y_{max} and y_{min} are the maximum and minimum values of Y within each segment. A more clear explanation of the difference between *LS* and *RLS* is indicated in Fig. 5.

LS divides the entire cluster into several segments. The density of points within each segment is similar if the segment belongs to the road. On the contrary, if the segment contains the road curb, the point density will increase. *RLS* is the real length of the segment. This parameter is set because of the discontinuous distribution of points. Points on the road are evenly distributed, so the *RLS* is quite close to the *LS*. But for the segment that contains the curb points, points are concentrated at the location of the curb. So the *RLS* may be smaller than the *LS*. In conclusion, the *LS* is only responsible for dividing the data into segments, and the point density within the segment is actually determined by the *RLS*.

After the division of segments, the number of points within each segment can also be calculated. Therefore, the point density of each segment can be easily achieved using,

$$SPD = \frac{segmentsize}{RLS} \tag{3}$$

where, SPD is the segment point density, $segmentsize$ is the number of points within one segment. Now the mean $Mean$ and standard deviation of segments SV can be calculated by,

$$Mean = \frac{\sum SPD}{NS} \tag{4}$$

$$SV = \sqrt{\frac{\sum (SPD - Mean)^2}{NS - 1}} \tag{5}$$

where, NS is the number of segments within each cluster. According to the 68-95-99.7 (Empirical) Rule or 3-Sigma Rule, about 68.27%, 95.45% and 99.73% of the values are lie within one, two and three standard deviations of the mean, respectively, in a normal distribution [22]. Thus, values of segment point density beyond the observation range $[Mean - 3 * SV, Mean + 3 * SV]$ are considered as noises. Algorithm 1 shows the detail of this procedure.

Algorithm 1 Curb Points Detection

Input: data of each cluster, LC-length of clusters
Output: cloud_road data
LS- length of segments = 0.4m, NS- number of segments, RLS- real length of segments,
LMI- minimum limitation, segmentsize- number of points within each segment,
SPD- segment point density, LMA- maximum limitation, si- current segment number,
SV- standard deviation for segments, Mean- mean of point number for segments
for each cluster **do**
  $NS = (LC/LS) + 1$
  for $si < NS$ **do**
    if $points.y \leq max\_y - si*LS \;\&\&\; points.y \geq max\_y - (si+1)*LS$
      $RLS = max\_y - min\_y$
      $SPD = segmentsize/RLS$
    end if
  end for
  $Mean = (\sum SPD)/NS$
  $SV = \sqrt{(\sum (SPD - Mean)^2)/(NS - 1)}$
  $LMI = Mean - 3*SV$, $LMA = Mean + 3*SV$
  for each segment **do**
    if $SPD \geq LMI \;\; SPD \leq LMA$
      add points in this segment to cloud_road data
    end if
  end for
end for
return cloud_road data

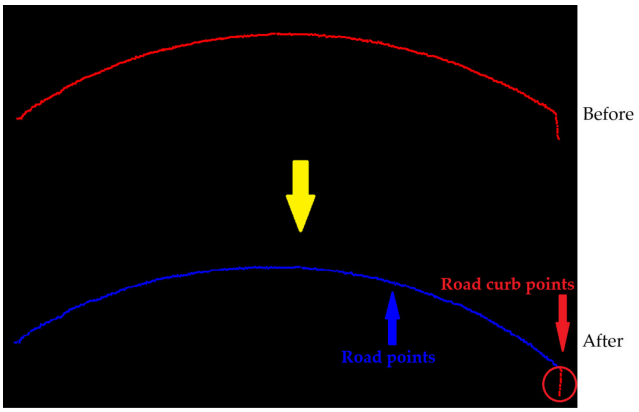

FIGURE 6. A comparison before and after the road curb detection: red points in the first row are rough road; blue points in the second row are road, and points in red are road curb data.

Fig. 6 shows the comparison result of before and after the operation of the curb detection algorithm. Here, the red points in the first row are rough road points. The second row of that figure indicates the results of the road curb points detection algorithm. Points in blue are the recognized road points, while red points are road curb points that will be ignored in the next procedure of lane marking identification. Therefore, Fig. 6 shows that points representing roadside curbs are successfully filtered, and road surface data are preserved.

B. LANE MARKING IDENTIFICATION AND REFINEMENT

It is quite usual that the reflectivity of white color objects, such as road markings, is higher than in black, such as asphalt. As the lane markings are made of high reflectivity materials, so the intensity values of lane marking points are higher than asphalt pavement points. Therefore, those markings can be identified using the intensity value of such points. However, intensity information preserved by LiDAR sensors, varies greatly even in the same longitudinal position between different scan lines because of the influence of distance, angle, or road geometry [23], as illustrated in Fig. 7(a). In this figure, X and Y are distance information, Z is the echo intensity. The positive direction of the X-axis is the driving direction, and road points are symmetrically distributed along the Y-axis. There are 6 points with high-intensity values for three scan lines are marked as A, B, C, D, E, F. Fig. 7(b) is the bird eye view (BEV) of Fig. 7(a). It can show the positional relationship of these 6 points more clearly. Y values of points A, B, and C or the other three points D, E, and F are similar. However, the difference in intensity values is quite large. For example, the difference in intensity between A and B is about 20. So, we can conclude that even in the same longitudinal position of different scan lines, the intensity information differs. To solve the above issues, an adaptive threshold selection method is proposed in this paper, and the corresponding results show the successful recognition of lane marking points.

As mentioned in the previous section, curb points are filtered and pavement points are sorted out based on scan

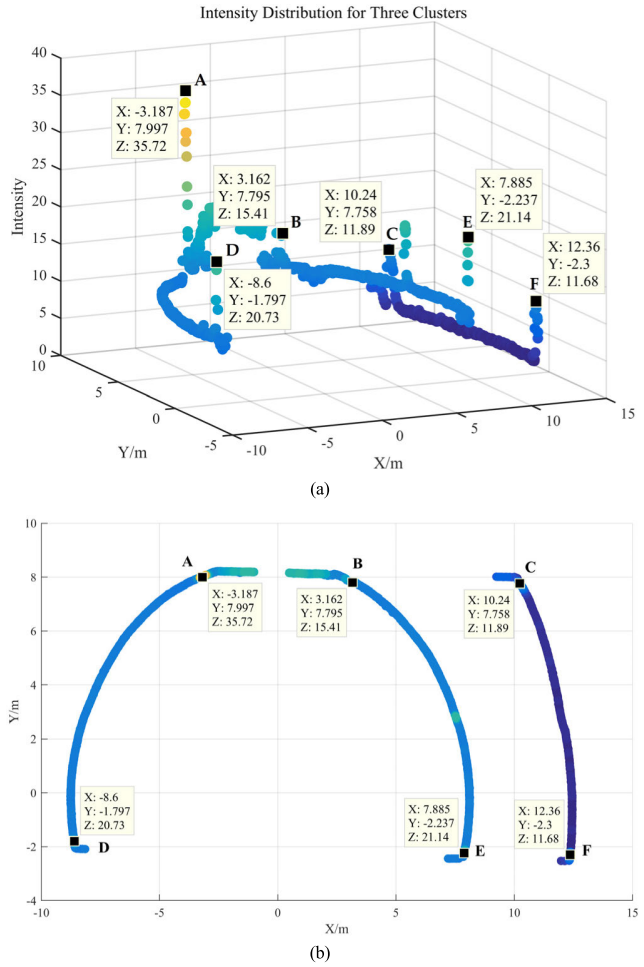

FIGURE 7. Intensity distribution: (a) intensity distribution for three clusters, (b) the BEV of the intensity distribution for three clusters.

lines after implementing constrained RANSAC algorithm and curb filtering algorithm based on segment point density. Hence, lane marking points can be distinguished from road clouds based on their features within each scan line instead of setting a global threshold [24] or an intensity band [25]. Algorithm 2 shows the detailed description of the proposed adaptive threshold selection approach. In this method, the linearity gray transform is first applied to unify intensity values within each scan line to k: [0, 255] by using (6).

$$grayvalue_j = \frac{(grayscale - 1) * intensity_j}{max\_intensity_i} \tag{6}$$

where, $grayvalue_j$ is the transformed gray value of point j, $grayscale$ equals 256, $intensity_j$ is the original intensity value of point j, $max\_intensity_i$ is the maximum intensity value of scan line i. And calculate the global average gray value ave

$$ave = \frac{\sum_{j=0}^{clustersize_i} grayvalue_j}{clustersize_i} \tag{7}$$

where $clustersize_i$ is the number of points within scan line i. Count the number $num_{grayvalue>ave}$ of points with gray values higher than the global average gray value ave. And calculate the mean value $ave0$ of those points.

$$ave0 = \frac{\sum_{grayvalue>ave} grayvalue_j}{num_{grayvalue>ave}} \tag{8}$$

Then, calculate probabilities p_k for each gray level.

$$p_k = \frac{num\_k}{clustersize_i} \tag{9}$$

where, num_k is the number of points with gray value k within scan line i. Next, the mean value $ave0$ is set as the initial threshold, and the threshold interval is defined as [$ave0$, 255]. Therefore, the optimum threshold is determined by the following equations

$$\omega_{1i} = \sum_{k=ave0}^{th} p_k \tag{10}$$

$$\mu_{1i} = \frac{\sum_{k=ave0}^{th} kp_k}{\omega_{1i}} \tag{11}$$

where th is the current threshold, and points in scan line i with gray values higher than $ave0$ will be divided into two classes. Points with gray values higher than $ave0$ but smaller than th are class 1, while points with gray values belong to the range [th, 255] are class 2. So, ω_{1i} is the probability of class 1 for scan line i. μ_{1i} is the mean gray value of class 1 for scan line i. The following equation shows the inter-class variance.

$$\sigma_i^2 = \omega_{1i}\sigma_{1i}^2 + \omega_{2i}\sigma_{2i}^2 = \omega_{1i}(\mu_{1i} - \mu_{Gi})^2 + \omega_{2i}(\mu_{2i} - \mu_{Gi})^2 \tag{12}$$

In this equation, σ_i^2 is the inter-class variance of scan line i, and μ_{Gi} is the global mean. ω_{2i} is the probability of class 2, and μ_{2i} is the mean gray value of class 2. They use the same calculation equations as like class 1, where only the range of k is different.

The desired threshold is the value of th that maximizes the inter-class variance. Compared with the original Otsu's method [24] that determines the best possible threshold by stepping through integers from 0 to 255 as potential thresholds, this method reduces the number of calculations by about 200 for one scan line by using the redefined threshold selection interval. Besides, the best threshold determined by this method is more appropriate because of the reduction of interference from road points with lower gray values.

In addition, to further optimize the results of the adaptive threshold selection method, the RANSAC algorithm with a line model is performed to filter noises far away from lane markings in the driving direction. This approach is implemented based on the assumption that lane markings are organized regularly in the shape of straight or curved. The reason for using a model-based method is that it has good robustness when the lane markings are worn or blocked by obstacles [26]–[28].

Algorithm 2 Adaptive Threshold Selection Algorithm

Input: road_data
Output: cloud_candidate_points

grayscale = 256, grayvalue- gray values, clustersize- number of points within a cluster,
max_intensity- maximum intensity, ave- global average gray value, ave0- mean value,
intensity- intensities of points, p_k- probability of gray level k, th- current threshold,
Ω- probability of classes, μ- mean gray values of classes, threshold- optimal threshold
for each cluster **do**
  $grayvalue = (grayscale - 1)^* intensity / max\_intensity$
  $ave = \sum_{j=0}^{clustersize} grayvalue / clustersize$
  $ave0 = \sum_{grayvalue>ave} grayvalue / num_{grayvalue>ave}$
  $p_k = num\_k / clustersize$
  for th from ave0 to grayscale **do**
    $\omega_1 = \sum_{k=ave0}^{th} p_k \quad \mu_1 = \sum_{k=ave0}^{th} kp_k / \omega_1$
    $\omega_2 = \sum_{k=th+1}^{grayscale-1} p_k \quad \mu_2 = \sum_{k=th+1}^{grayscale-1} kp_k / \omega_2$
    $\mu_G = \sum_{k=ave0}^{grayscale-1} kp_k \quad \sigma^2 = \omega_1 (\mu_1 - \mu_G)^2 + \omega_2 (\mu_2 - \mu_G)^2$
    if max σ^2
      $threshold = th$
    end if
  end for
  if $grayvalue \geq threshold$
    add point with this grayvalue to cloud_candidate_points
  end if
end for
return cloud_candidate_points

IV. RESULTS AND DISCUSSION

A. REGION-OF-INTEREST

Fig. 8 shows the outcomes of the ROI selection approach that includes the results of the rough road data with marks of curb points as well as, the results using the curb filtering algorithm based on segment point density. Fig. 8(a) shows a frame of the original point clouds. The extraction of road surface data and its effect is displayed in Fig. 8(b). After operating the constraint RANSAC-plane algorithm, rough ground data are segmented from the whole point clouds. Here, the blue points are rough road data, while other objects are in red. It is clear that some curb points still exist as the result of road segmentation as shown in Fig. 8(c). The selected area is enlarged in a yellow box, where the circles indicate the positions of road curb points. Subsequently, the curb detection algorithm based on segment point density is carried out, and results are presented in Fig. 8(d). At this stage, the ROI selection of point clouds is completed, and ground points are well prepared for further processing.

B. QUALITATIVE RESULTS

The application of the adaptive threshold selection method and its results based on five datasets are presented in Fig. 9.

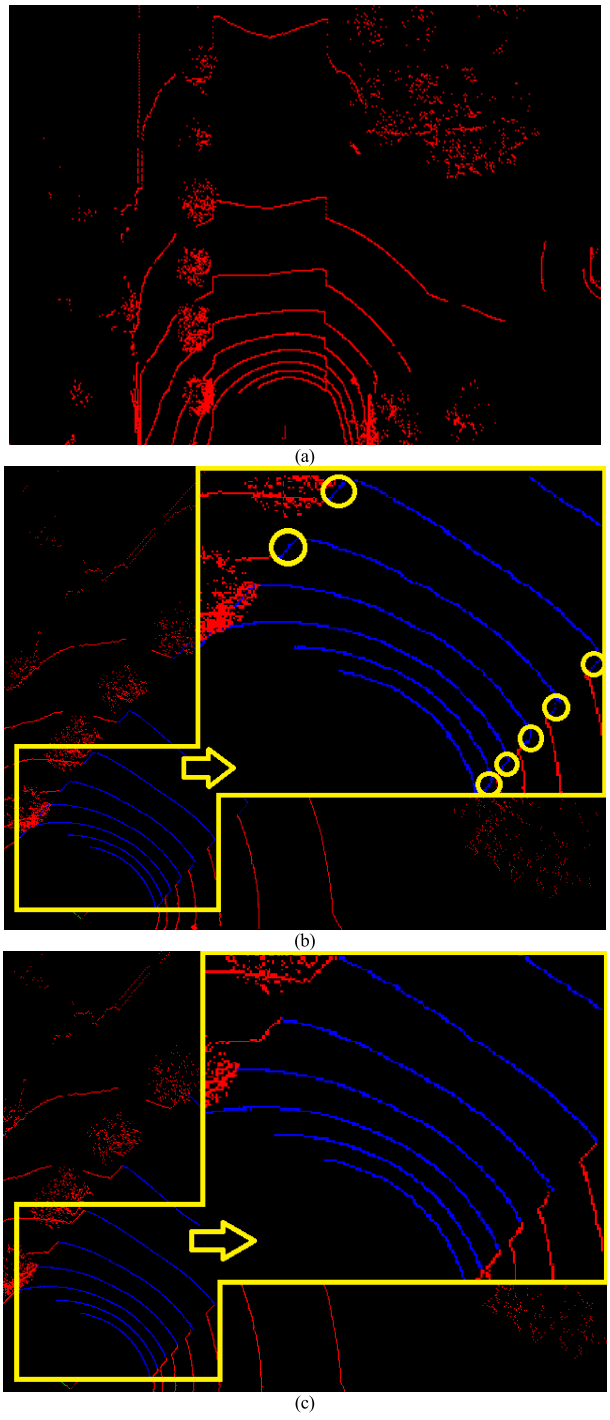

FIGURE 8. Results based on the ROI selection: (a) original data, (b) rough road data with curb points in yellow circles (inset shows the zoom-in of selected points), (c) results of final road data (inset shows the zoom-in of selected area).

Green, blue, and red points are identified as lane markings, road, and other objects, respectively. Fig. 9(a) is a sample of dataset 1, which is collected from an ideal structured road. It is a double-driving straight road without any slope. Fig. 9(b) is a sample from dataset 2 which is also collected from a flat double-driving straight road. The only difference is that there is a dashed white line in dataset 1 but a yellow

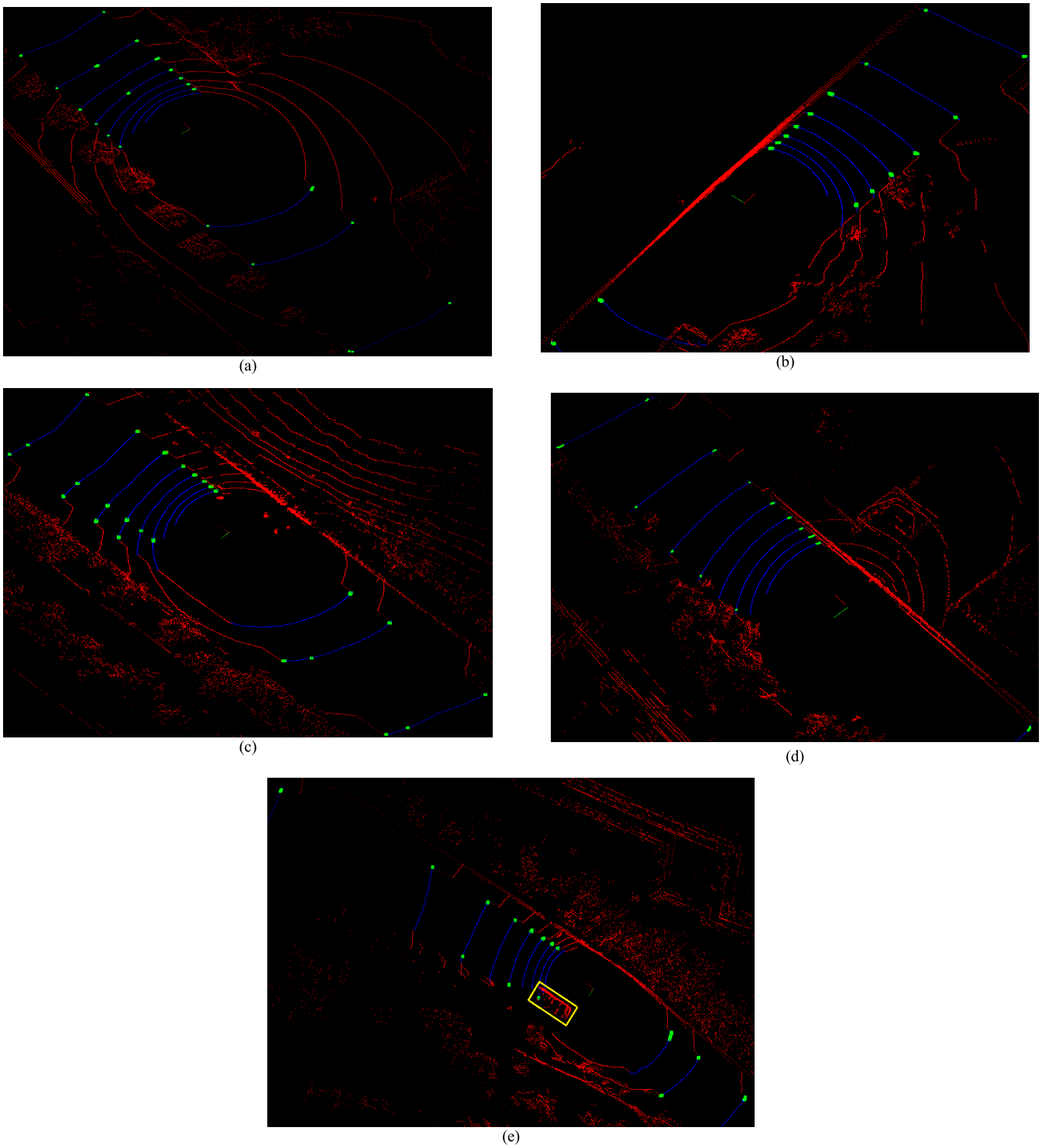

FIGURE 9. Results of lane marking detection: (a) a sample result of dataset 1, (b) a sample result of dataset 2, (c) a sample result of dataset 3, (d) a sample result of dataset 4, (e) a sample result of dataset 5.

solid line in dataset 2. Some parts of the white dashed line are in green. Due to the long gap between each scan line with data processing frame by frame, dashed lines cannot be fully recognized. Here, the two white solid lines are identified. Fig. 9(c) is the result of dataset 3, which is collected from an incline roadside parking lot with three white solid lines, which are successfully detected. A result of an uphill road with two solid lines is drawn in Fig. 9(d). In Fig. 9(e), the sample of an uphill curved road with two solid lane markings is presented. The yellow box marks a moving vehicle which

shows that the proposed method can determine the lane line points even some parts of lane markings are obscured. The experimental results justify that the model can successfully detect lane markings when the majority of lane marking points are recorded. Overall, the presented results show the effectiveness of the proposed algorithm of identifying lane markings under different road conditions.

C. QUANTITATIVE RESULTS

To evaluate the performance of the proposed lane marking detection algorithm, different performance metrics are investigated [29]. Here, four coefficients are commonly utilized: Precision, Recall, Dice, and Jaccard. The following equations are the corresponding definitions of performance metrics:

Precision represents the fraction of detected marking points that are true marking points. It reflects the correctness of the lane marking detection. The definition is as follows:

$$Precision = \frac{TP}{TP + FP} \tag{13}$$

where TP is the number of true positive points, which reflects the detected lane marking points are true lane marking points. FP is the number of false positive points, which is the detected lane marking points are actually road points.

Recall signifies the fraction of truly detected marking points, and it reflects the completeness of the lane marking detection. It defines as follows:

$$Recall = \frac{TP}{TP + FN} \tag{14}$$

where FN is the number of false negative points, which means that the undetected points are actually lane marking points.

Dice is the harmonic mean of Precision and Recall, and it quantifies the average performance. It defines as follows:

$$Dice = \frac{2^{*}Precision^{*}Recall}{Precision + Recall} \tag{15}$$

Jaccard manifests worst case performance. This metric defines as follows:

$$Jaccard = \frac{TP}{TP + FP + FN} \tag{16}$$

This evaluation is done by manually comparing with ground truth datasets. The width of lane markings is fixed, while the distance between two neighboring points is different for each scan line because of the different detection distances. But still, the number of points representing lane markings can be calculated. So, we can set different numbers of the true lane marking points for every scan line. The program is set to show the number of detected lane marking points to evaluate the performance metrics. Then the evaluation can be achieved. The quantitative evaluation results are recorded in Table 1. We select 200 frames of data from every dataset, randomly. So, this is an average evaluation table for the five datasets.

As shown in Table 1, the adaptive threshold selection method achieved Precision of 97.23%, 99.22%, 98.23%, 92.56%, and 85.23%; Recall of 84.04%, 81.91%, 87.39%, 90.97%, and 92.55%; Dice of 89.91%, 89.58%, 92.40%, 91.65%, and 88.48%; Jaccard of 82.06%, 81.41%, 85.98%, 84.76%, and 79.91% on the five datasets, respectively. The average Precision, Recall, Dice, and Jaccard for five datasets are 94.49%, 87.37%, 90.40% and 82.82%, respectively.

TABLE 1. Quantitative evaluation results.

	Precision	Recall	Dice	Jaccard
Dataset 1	97.23%	84.04%	89.91%	82.06%
Dataset 2	99.22%	81.91%	89.58%	81.41%
Dataset 3	98.23%	87.39%	92.40%	85.98%
Dataset 4	92.56%	90.97%	91.65%	84.76%
Dataset 5	85.23%	92.55%	88.48%	79.91%
Average	94.49%	87.37%	90.40%	82.82%

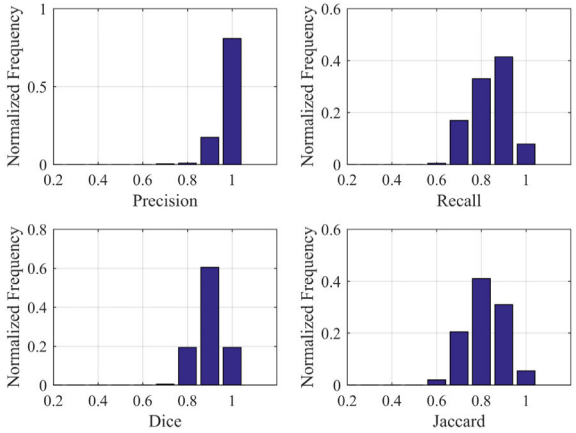

FIGURE 10. Histogram of evaluation coefficients for dataset 1: precision, recall, dice, and Jaccard.

In [29], quantitative results are based on the Dice coefficient and Jaccard index for four datasets, which are as follows. Dice coefficient: 77.80%, 55.90%, 71.33%, 66.23%, and Jaccard index are 66.38%, 43.22%, 58.66%, 54.82%. In comparison, based on our proposed model using five datasets, the Dice coefficient and Jaccard index are as follows. Dice coefficient: 89.91%, 89.58%, 92.40%, 91.65%, 88.48%, and Jaccard index: 82.06%, 81.41%, 85.98%, 84.76%, 79.91%. Results of Dice and Jaccard confirm that the proposed method outperforms the results as appeared in [29], where a similar 16-beam-LiDAR has been used for investigation.

The comparison of dataset 1 and dataset 2 shows that white lines can be detected, even some parts of the dashed line. The results of dataset 3 clarify that a little slope will enhance the detection quality of lane markings, compared with the flat road in dataset 1. But if the slope is too high, as the uphill in dataset 4, the quality can be affected. The comparison of results of dataset 5 and dataset 4 shows that the curvature of roads does influence the quality of detection.

Fig. 10 to Fig. 14 present the histogram of Precision, Recall, Dice and Jaccard coefficients for the respective five

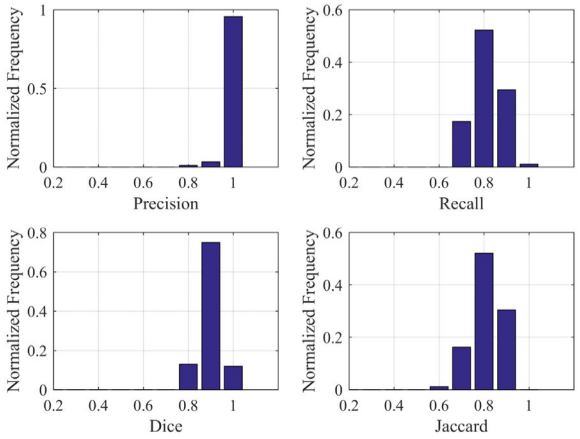

FIGURE 11. Histogram of evaluation coefficients for dataset 2: precision, recall, dice, and Jaccard.

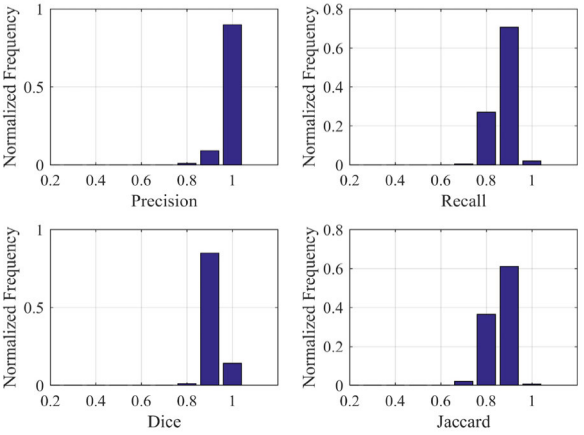

FIGURE 12. Histogram of evaluation coefficients for dataset 3: precision, recall, dice, and Jaccard.

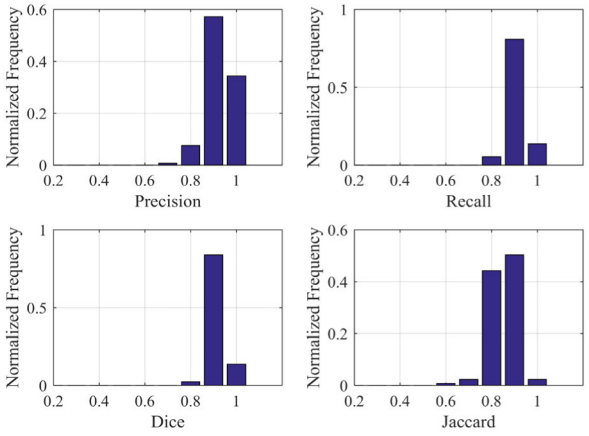

FIGURE 13. Histogram of evaluation coefficients for dataset 4: precision, recall, dice, and Jaccard.

datasets. The occurrence frequency is normalized so that the sum of heights of all bars equals 1.

Table 2 lists the average detection distance of the adaptive threshold selection method for 200 frames data from every dataset. Since this method process data frame by frame,

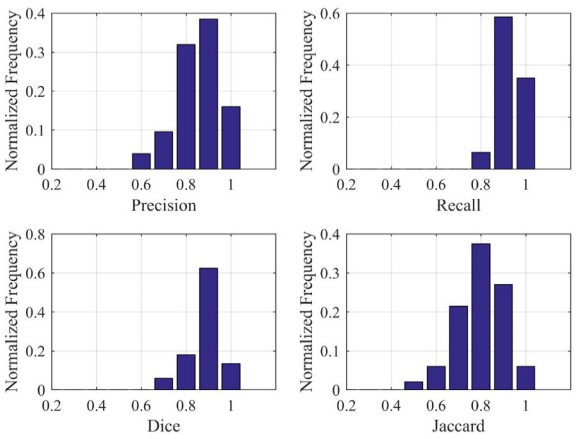

FIGURE 14. Histogram of evaluation coefficients for dataset 5: precision, recall, dice, and Jaccard.

TABLE 2. Detection distance.

	Dataset 1	Dataset 2	Dataset 3	Dataset 4	Dataset 5
Distance/m	47.14	33.52	42.41	33.01	38.31

TABLE 3. Computation time.

	Rough road data extraction/ms	Lane marking points identification/ms	Total/ms
Dataset 1	7.20	38.70	45.90
Dataset 2	3.35	29.07	32.42
Dataset 3	1.51	31.50	33.01
Dataset 4	4.51	32.17	36.68
Dataset 5	3.37	25.07	28.44

the detection range shown in Table 2 is the average distance per frame. The average detection distance for the five datasets is 47.14 m, 33.52 m, 42.41m, 33.01 m, and 38.31 m, respectively.

The curb filtering and lane marking identification algorithm proposed in this research is written in C++ and operated on an Intel Core i5-1035G7 computer in the Linux system. The computation time of five datasets for extracting rough road points and detecting lane marking points are stated in Table 3. The time used for lane marking detection for the five datasets is 38.70 ms, 29.07 ms, 31.50 ms, 32.17 ms, and 25.07 ms, respectively. The total running time is no more than 50 ms per frame. This fast response time is quite effective for lane marking detection especially using LiDAR sensors in autonomous driving. As stated before, many researchers used LiDAR to develop digital road maps, and thus the computational time is not a primary factor to consider for their investigation.

According to the regulations of speed limitation, the maximum speed on the expressway cannot exceed 120 km/h,

which is 33.3 m/s. Therefore, the proposed method could detect lane markings reach at least 33 m within 50 ms. Hence, the presented results justify the use of the proposed method for the detection of lane marking in real-time.

However, there are still some opportunities to improve the presented results such as the full identification of dashed lines and yellow lines. The quantitative evaluation results still need to be improved. After all, safety is of paramount importance. Besides, other markings play a significant role in guiding the behavior of vehicles as well. Our future direction will focus on solving these issues.

V. CONCLUSION

An efficient method with real-time operation was proposed in this research to filter curb points and detect lane markings on the structured roads from 3D point clouds operated by cost-effective 16-beam LiDAR. The overall system includes two sections: ROI selection and lane marking identification. In the ROI selection, a constrained RANSAC algorithm, and the newly designed curb detection approach based on segment point density were applied to achieve the road data segmentation and refinement. Additionally, in the lane marking recognition part, an adaptive threshold selection method was implemented to distinguish marking points from ground point clouds and reduce the computation time. The proposed method was tested for five datasets with diverse road conditions as prepared by our research laboratory. Moreover, the quantitative results were evaluated by performance metrics like Precision, Recall, Dice, and Jaccard. Here, the average results for five datasets are 94.49%, 87.37%, 90.40%, and 82.82%, respectively. Also, the average detection range for a frame is 47.14 m, 33.52 m, 42.41 m, 33.01 m, and 38.31 m, respectively. In addition, the average computation time is no more than 50 milliseconds per frame, which eventually shows the efficient operation on a real-time basis of the proposed method.

REFERENCES

[1] *Let the Races Begin: Helping the Next Generation Discover Self-Driving*. Accessed: May 11, 2021. [Online]. Available: https://blog.waymo.com/2019/09/let-races-begin-helping-next-generation.html
[2] *Hyundai Motor Announces Open Innovation Partnership With Brown University to Enhance Future Mobility*. Accessed: May 11, 2021. [Online]. Available: https://www.hyundainews.com/en-us/releases/2654
[3] D. Feng, C. Haase-Schütz, L. Rosenbaum, H. Hertlein, C. Gläeser, F. Timm, W. Wiesbeck, and K. Dietmayer, "Deep multi-modal object detection and semantic segmentation for autonomous driving: Datasets, methods, and challenges," *IEEE Trans. Intell. Transp. Syst.*, vol. 22, no. 3, pp. 1341–1360, Mar. 2021.
[4] W. Liu, F. Yan, J. Zhang, and T. Deng, "A robust lane detection model using vertical spatial features and contextual driving information," *Sensors*, vol. 21, no. 3, p. 708, Jan. 2021.
[5] Q. Zou, H. Jiang, Q. Dai, Y. Yue, L. Chen, and Q. Wang, "Robust lane detection from continuous driving scenes using deep neural networks," *IEEE Trans. Veh. Technol.*, vol. 69, no. 1, pp. 41–54, Jan. 2020.
[6] Z. Liu, Y. Cai, H. Wang, L. Chen, H. Gao, Y. Jia, and Y. Li, "Robust target recognition and tracking of self-driving cars with radar and camera information fusion under severe weather conditions," *IEEE Trans. Intell. Transp. Syst.*, early access, Feb. 24, 2021, doi: 10.1109/TITS.2021.3059674.
[7] O. Schumann, J. Lombacher, M. Hahn, C. Wöhler, and J. Dickmann, "Scene understanding with automotive radar," *IEEE Trans. Intell. Veh.*, vol. 5, no. 2, pp. 188–203, Jun. 2020.
[8] H. Guan, J. Li, Y. Yu, C. Wang, M. Chapman, and B. Yang, "Using mobile laser scanning data for automated extraction of road markings," *ISPRS J. Photogramm. Remote Sens.*, vol. 87, pp. 93–107, Jan. 2014.
[9] H. Guan, J. Li, Y. Yu, Z. Ji, and C. Wang, "Using mobile LiDAR data for rapidly updating road markings," *IEEE Trans. Intell. Transp. Syst.*, vol. 16, no. 5, pp. 2457–2466, Oct. 2015.
[10] Y.-T. Cheng, A. Patel, C. Wen, D. Bullock, and A. Habib, "Intensity thresholding and deep learning based lane marking extraction and lane width estimation from mobile light detection and ranging (LiDAR) point clouds," *Remote Sens.*, vol. 12, no. 9, p. 1379, Apr. 2020.
[11] L. Ma, Y. Li, J. Li, Y. Yu, J. M. Junior, W. N. Gonçalves, and A. M. Chapman, "Capsule-based networks for road marking extraction and classification from mobile LiDAR point clouds," *IEEE Trans. Intell. Transp. Syst.*, vol. 22, no. 4, pp. 1981–1995, Apr. 2021.
[12] Y. Yu, J. Li, H. Guan, F. Jia, and C. Wang, "Learning hierarchical features for automated extraction of road markings from 3-D mobile LiDAR point clouds," *IEEE J. Sel. Topics Appl. Earth Observ. Remote Sens.*, vol. 8, no. 2, pp. 709–726, Feb. 2015.
[13] L. Yan, H. Liu, J. Tan, Z. Li, H. Xie, and C. Chen, "Scan line based road marking extraction from mobile LiDAR point clouds," *Sensors*, vol. 16, no. 6, p. 903, Jun. 2016.
[14] J. Jung and S.-H. Bae, "Real-time road lane detection in urban areas using LiDAR data," *Electronics*, vol. 7, no. 11, p. 276, Oct. 2018.
[15] S. Kammel and B. Pitzer, "LiDAR-based lane marker detection and mapping," in *Proc. IEEE IVS*, Eindhoven, The Netherlands, Jun. 2008, pp. 1137–1142.
[16] F. Xu, L. Chen, J. Lou, and M. Ren, "A real-time road detection method based on reorganized LiDAR data," *PLoS ONE*, vol. 14, no. 4, Apr. 2019, Art. no. e0215159.
[17] F. Ghallabi, F. Nashashibi, G. El-Haj-Shhade, and M.-A. Mittet, "LiDAR-based lane marking detection for vehicle positioning in an HD map," in *Proc. ITSC*, Maui, HI, USA, Nov. 2018, pp. 2209–2214.
[18] H. Kim, B. Liu, and H. Myung, "Road-feature extraction using point cloud and 3D LiDAR sensor for vehicle localization," in *Proc. URAI*, Jeju, South Korea, Jun. 2017, pp. 891–892.
[19] G. Wang, J. Wu, R. He, and S. Yang, "A point cloud-based robust road curb detection and tracking method," *IEEE Access*, vol. 7, pp. 24610–24625, 2019.
[20] L. Smadja, J. Ninot, and T. Gavrilovic, "Road extraction and environment interpretation from LiDAR sensors," *IAPRS*, vol. 38, pp. 281–286, Sep. 2010.
[21] RoboSense. *RS-LiDAR-16 User Manual V4.3.3 (English)*. Accessed: Feb. 9, 2021. [Online]. Available: https://www.robosense.cn/resources-27
[22] *68-95-99.7 Rule*. Accessed: May 17, 2021. [Online]. Available: https://en.wikipedia.org/wiki/68-95-99.7_rule
[23] J. Jeong and A. Kim, "LiDAR intensity calibration for road marking extraction," in *Proc. UR*, Honolulu, HI, USA, Jun. 2018, pp. 455–460.
[24] A. Hata and D. Wolf, "Road marking detection using LiDAR reflective intensity data and its application to vehicle localization," in *Proc. ITSC*, Qingdao, China, Oct. 2014, pp. 584–589.
[25] Y.-F. Wang and Y.-S. Tsai. *A Lane Detection Method Based on 3D-LiDAR*. Accessed: Apr. 14, 2021. [Online]. Available: https://www.artc.org.tw/upfiles/ADUpload/knowledge/tw_knowledge_598788766.pdf
[26] J. Wang, Y. Chen, J. Xie, and H. Lin, "Model-based lane detection and lane following for intelligent vehicles," in *Proc. ICIHMSC*, Nanjing, China, Aug. 2010, pp. 170–175.
[27] H. Wang, Y. Wang, X. Zhao, G. Wang, H. Huang, and J. Zhang, "Lane detection of curving road for structural highway with straight-curve model on vision," *IEEE Trans. Veh. Technol.*, vol. 68, no. 6, pp. 5321–5330, Jun. 2019.
[28] J. Yoo and D. Kim, "Graph model-based lane-marking feature extraction for lane detection," *Sensors*, vol. 21, no. 13, pp. 1–21, Jun. 2021.
[29] L. D. P. Veronese, A. Ismail, V. Narayan, and M. Schulze, "An accurate and computational efficient system for detecting and classifying ego and sides lanes using LiDAR," in *Proc. IEEE IV*, Suzhou, China, Jun. 2018, pp. 1476–1483.

JING HUANG received the B.S. degree in communication engineering from the Shandong University of Science and Technology, Qingdao, China, in 2017, the M.S. degree in information and communication engineering from the Chongqing University of Technology, Chongqing, China, and the M.S. degree in electrical engineering from the Korea Advanced Institute of Science and Technology, Daejeon, South Korea, in 2021, where she is currently pursuing the Ph.D. degree in electrical engineering. Her research interests include automated vehicles, lane detection, and curb detection by using LiDAR point clouds.

PALLAB K. CHOUDHURY (Member, IEEE) received the B.Sc. degree in electrical and electronic engineering from the Khulna University of Engineering & Technology (KUET), Khulna, Bangladesh, in 2003, the M.S. degree in information and communication technologies from the Asian Institute of Technology, Thailand, in 2007, and the Ph.D. degree in optical communication engineering from the Integrated Research Center for Photonics Networks and Technologies (IRCPhoNET), Scuola Superiore Sant'Anna, Pisa, Italy, in 2012. From 2012 to 2013, he was a Research Assistant with the Research Group of Optical System Design, IRCPhoNET. From 2018 to 2019, he worked as a Postdoctoral Fellow with the LiDAR and Intelligent Optical Node (LION) Research Laboratory, jointly formed by the Chongqing University of Technology (CQUT), Chongqing, China, and the Korea Advanced Institute of Science and Technology (KAIST), Daejeon, South Korea. He is currently a Professor with the Department of Electronics and Communication Engineering, KUET. He is the author of more than 40 international journals and conferences. He also holds one U.S. patent. His research interests include the design and development of LiDAR for autonomous vehicle, computational imaging optics, optical wireless transmission, passive optical networks, and application of multi-level modulation formats like OFDM. He is an Associate Editor of IEEE Access.

SONG YIN received the B.S. degree in communication engineering from the Nanjing University of Posts and Telecommunications, Nanjing, China, in 2017. She is currently pursuing the M.S. degree in information and communication engineering with the Chongqing University of Technology, Chongqing, China, and the M.S. degree in electrical engineering with the Korea Advanced Institute of Science and Technology, Daejeon, South Korea. Her research interest includes the detection of unstructured road boundaries based on LiDAR point clouds.

LINGYUN ZHU received the B.S. degree in welding equipment and technology, the M.S. degree in welding automation, and the Ph.D. degree in control theory and control engineering from the Chongqing University, Chongqing, China, in 1992, 2000, and 2003, respectively. From March 2015 to September 2015, he was a Visiting Scholar at the Department of Computer Science, Korea Advanced Institute of Science and Technology, Daejeon, South Korea. He is currently an Associate Professor with the Liangjiang International College, Chongqing University of Technology, Chongqing. He has authored or coauthored two books, more than 30 articles, five patents, and has been in charge of or participated in 11 research projects funded by the national government or institutional organizations. His research interests include intelligent perception of human physiological information, automated vehicles, and computer vision.